Quench Level of the HL-LHC Nb_3Sn IR quadrupoles

Marco Breschi, Enrico Felcini, Luca Bottura

***Abstract*— The scope of the Large Hadron Collider Hi-Lumi Project at CERN includes the installation of several superconducting magnets wound with Nb_3Sn Rutherford cables. The quench level of these magnets (i.e. the maximum energy that a cable can tolerate without quenching) is a key value required to set magnet protection from beam losses, and is expected to be significantly different from the computed and measured levels of the LHC Nb-Ti magnets. In this work, we applied a one-dimensional numerical model of multi-strand Rutherford cables to simulate the electro-thermal instabilities caused by the heat released by the particle beam losses. Two models have been applied, one based on the analysis of the single strand, and the other accounting for all the strands in the multi-strand cable. The results of these two models are compared to analyze the effects of heat and current redistribution during quench. A comparison between the quench energy values obtained for the Nb_3Sn conductor in the working conditions of the LHC Hi-Lumi inner triplet low-β quadrupole (MQXF) and those of the NbTi Rutherford cable of the LHC main quadrupole magnet (MQ) is presented. The differences and similarities in quench performance between the impregnated cables for Nb_3Sn magnets and the non-impregnated ones for NbTi magnets at their respective typical working conditions in superconducting accelerator magnets are highlighted.**

***Index Terms*—Nb_3Sn Rutherford cables, Quench, Beam Loss, Electro-thermal modeling, Accelerator magnets.**

I. Introduction

The High Luminosity LHC (HL-LHC) project is aimed at implementing the necessary changes in the LHC to increase its integrated luminosity by a factor ten [1], [2]. Among the magnets that will be replaced are the 16 superconducting inner triplet (low-β) quadrupoles placed around the two high luminosity interaction regions (ATLAS and CMS experiments). Control and prevention of the transition from superconducting state to the normal one, referred as *quench*, is one of the most important and thorny problems concerning the safe operation of accelerator magnets.

As described in [3], one of the main heat disturbances is generated by the impact on superconducting wires of a shower of secondary particles generated by the collisions of the protons that escape from the collimated beam. Investigations on the impact of the beam losses on accelerator magnets in operation were presented in [4-10]. In the LHC machine, the deposited energy is measured by Beam Loss Monitors installed outside the magnet cryostats [11], aimed to predict a beam induced quench and dump the beam in case of disturbance levels exceeding prescribed thresholds. A correct setting of these thresholds, based on the computation of the magnet quench energy, allows avoiding unnecessary magnet quench.

In [12] the NbTi Rutherford cable was represented through a one-strand model described by a lumped parameter non-linear circuit, accounting for the non-uniform distribution of the interstitial helium across the cable width. In other analyses, also focused at NbTi magnets, the impact of the heat and current distribution between strands was studied with a distributed parameter model accounting for all the strands in the cable [13].

This work extends the previous analyses to study the electro-thermal behavior of the Nb_3Sn Rutherford cables presently under development for the HL-LHC project. The numerical model, implemented in the THEA code [14], describes the cable and the helium bath in the magnet by means of a one-dimensional approach. Since the Nb_3Sn magnet is impregnated with epoxy resin, the interstitial spaces are filled with this insulating material. The longitudinal periodic variation of the heat deposition and of the magnetic flux density along each strand are taken into account. A quantitative assessment of the temperature and current imbalance between strands occurring during quench was performed. The quench energies of the Nb_3Sn conductor at the working conditions of the HL-LHC inner triplet low-β quadrupole (MQXF) have been computed as a function of heat pulse durations and operation current. These results are compared here with those obtained for the NbTi Rutherford cable of the LHC main quadrupole magnet (MQ) [13].

II. 1D Model Description

The analyses presented here are focused on the inner layer middle plane cable of the HL-LHC inner triplet low-β quadrupole (MQXF) shown in Fig. 1 [15] and Fig. 2 [16]. The main geometric parameters of the 40-strand Rutherford cable are presented in Table I. The *E-J* electric characteristics of each superconductive strand is described by the power law

$$\frac{E}{E_c} = \left(\frac{J}{J_c\left(B,T,\varepsilon\right)} \right)^n \qquad (1)$$

where the J_c (B, T, ε) dependence on magnetic flux density B, temperature T and strain ε is in the form adopted for all ITER strands [17]; the Nb_3Sn and its resistive stabilizer are assumed in parallel electrical connection. The strain of the

Manuscript received September 10, 2016.

M. Breschi is with the Department of Electrical, Electronic and Information Engineering of the University of Bologna, Bologna, 40136, Italy (phone +39-0512093584; fax: +390512093588; e-mail: marco.breschi@unibo.it).

E. Felcini is with the Department of Electrical, Electronic and Information Engineering of the University of Bologna, Bologna, 40136, Italy and with the TE Department, CERN, Geneva, Switzerland (e-mail: enrico.felcini@gmail.com)

L. Bottura is with the TE Department, CERN, Geneva, Switzerland (e-mail: luca.bottura@cern.ch).

superconducting filaments is assumed uniform along the length of the wires and set to −0.2 %. The total cable length is set to 4 m and the heat deposition, constant in time, but non-uniform in space, is applied to half of the cable length, at the center of the cable. Thanks to symmetry conditions, only half of the cable is simulated (length of 2 m), by imposing an adiabatic wall boundary condition at the left boundary. A constant temperature is set at the right boundary of the cable, under the assumption that the helium bath is a thermal reservoir at 1.9 K. The magnetic flux density is taken non-uniform along the cable; its distribution on the magnet cross section is computed with the ROXIE code [18] and is shown in Fig. 2 for the nominal current of 16470 A. The field profile along each wire exhibits oscillations with a period equal to the cable twist pitch (L_p), since all strands pass alternatively from the close vicinity to the magnet bore (maximal field) to the opposite side of the cable (minimal field). Similarly, the heat deposition due to beam losses, computed here with the FLUKA code [19], is characterized by consecutive decays and increases of the flux with period L_p along each strand axis. The cable simulations were performed by means of two distinct approaches, a 1-strand and a 40-strand model, described in detail in the following sections.

TABLE I
MQXF V.2 CABLE DATA

Parameter	Value
Cable Type	MQXF v.2
Strand diameter [mm]	0.85
Cu/non Cu ratio	1.2
Number of strands	40
Thin edge [mm]	1.462
Thick edge [mm]	1.588
Transposition pitch [mm]	109
Width [mm]	18.15

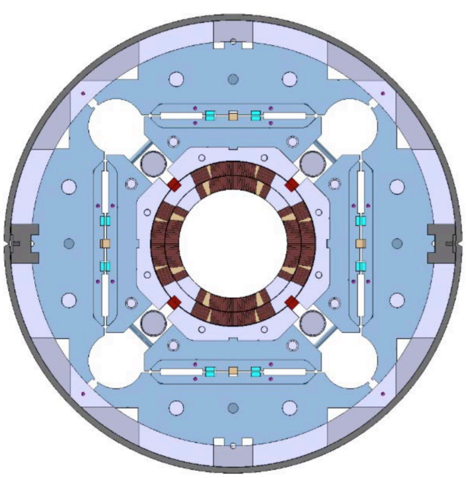

Fig. 1. Cross-section of the magnet MQXF for the Hi-Lumi LHC Project [15].

A. 1 strand model

The Rutherford cable made of N_s strands is modeled through only one strand, represented by means of a 1D thermo-electric model implemented in the THEA code [14]. The thermal elements considered in this analysis are the strand and the epoxy resin. The strand cannot exchange current and heat with the neighboring ones, and is surrounded by epoxy resin with an area equal to a fraction $1/N_s$ of the insulator spread in the cable cross section. The epoxy resin in turn is assumed in contact with the helium bath. No direct contact between strand and helium bath is taken into account. The following equation describes the thermal model of the strand

$$A_i \rho_i C_i \frac{\partial T_i}{\partial t} - \frac{\partial T_i}{\partial x}\left(A_i k_i \frac{\partial T_i}{\partial x}\right) = \dot{q}'_{St} + \dot{q}'_{Joule} + \sum_{j=1, j\neq i}^{N} \frac{(T_j - T_i)}{H_{ij}} + p_{He} h_{He}(T_{He} - T_{GE}) \quad (2)$$

where for each thermal component at temperature T_i, the terms A_i, ρ_i, C_i and k_i represent area of the cross section, density, specific heat, and thermal conductivity respectively. On the r.h.s, $\dot{q}'_{St}$ is the external heat introduced in the strand, $\dot{q}'_{Joule}$ the heat input due to Joule losses, H_{ij} the thermal resistance between the i^{th} and j^{th} elements, p_{HE} the wetted perimeter and h_{HE} the heat transfer coefficient between the epoxy resin and the helium bath.

B. Multi-strand model

This model accounts for all cable strands, connected to each other trough contact conductances and mutual inductances [20]. A parametric analysis was performed to assess the impact of the electric contact resistances. The values of $R^c_{h,k}$ were varied in the range from 1 μΩ to 100 μΩ keeping a constant ratio between $R^a_{h,k}$ and $R^c_{h,k}$. This ratio was set to 8 considering the measurements on the NbTi Main Quadrupole cable ($R^a_{h,k}$ = 320 μΩ and $R^c_{h,k}$ = 40 μΩ, see [21]). The formulae for the self-inductance of a straight cylindrical conductor, and for the mutual inductance of two parallel filiform conductors were taken from [22]. Thermal conductances per unit contact area for adjacent and non-adjacent strands were set to 5000 and 2500 W/m^2K respectively [21].

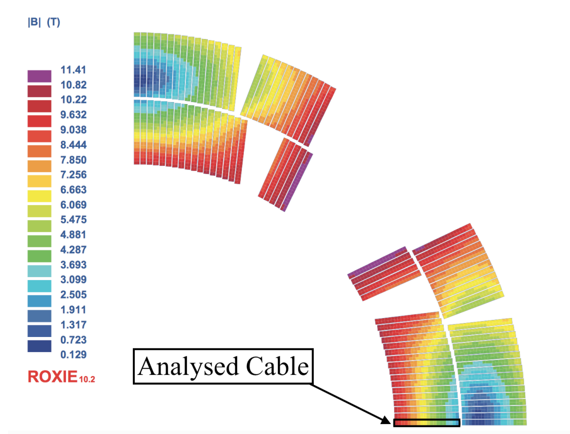

Fig. 2. Magnetic flux density in the cross section of the HL-LHC MQXF computed for a 16470 A operation current. The analyzed cable is the mid-plane inner layer one. The computations were performed with ROXIE [18].

C. Comparison between state of the art Nb_3Sn and NbTi Rutherford cables

A comparison between the main geometric parameters and working conditions of the mentioned MQXF cable and the NbTi cable for the Main Quadrupole (MQ) of the LHC machine, taken as representative of an accelerator magnet wound with NbTi, is presented in Table II. It is worth noting that, despite the higher magnetic field and transport current at nominal conditions of the Nb_3Sn magnet, the ratio of transport current to critical current is very similar for both magnets.

TABLE II
COMPARISON BETWEEN MQXF NB_3SN AND MQ NBTI CABLES

Parameter	Value	
Cable Type	MQXF Nb_3Sn	MQ NbTi
Strand diameter [mm]	0.850	0.825
Cu/non Cu ratio	1.20	1.95
Number of strands	40	36
Width [mm]	18.15	15.1
Total Current [kA]	16.47	11.87
Peak Magnetic Field	11.4	6.85
J_T/J_c	0.472	0.465
Temperature Margin	5.34	2.89

III. RESULTS AND DISCUSSION

Temperature and current redistribution

The simulations reported in this section were performed with the N_s-strand model, at the nominal working conditions of the Nb_3Sn MQXF magnets. The imposed disturbance duration was set to 10 μs. Only the temperature and current of one strand is shown in Fig. 3, which is representative for the similar behavior of all strands. As shown in Fig. 3a), the strand temperature exhibits 'traces' of the heat deposition on the strand, even at 0.1 s after the end of the external disturbance.

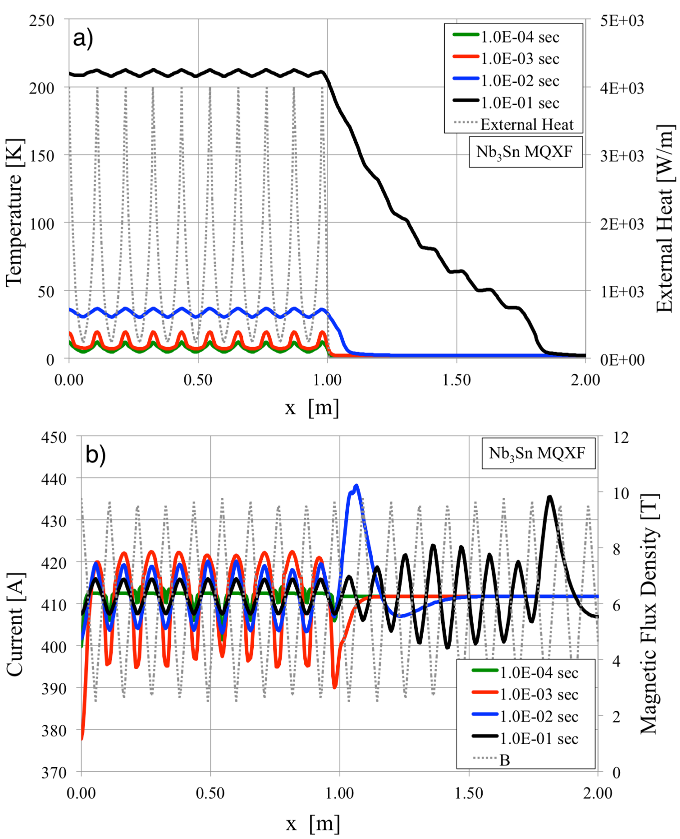

Fig. 3. a) Temperature and b) current distribution at different times after a 10 µs heat deposition for the Nb_3Sn cable of the HL-LHC MQXF, shown with the external heat deposition and magnetic flux density respectively

The temperature of the cable reaches quickly very high values, due to the poor heat connection between the strands and the helium bath. As for the current distribution, shown in Fig.3 b), one can observe a 'counter-phase' behavior with respect to the magnetic flux density, with minimal values of the current corresponding to the peaks of magnetic flux density. At these locations, the high electric fields determine in fact a redistribution of the current towards the neighboring strands. The quench propagation along the strand length can be observed through the temperature increase in Fig. 3a, and the initiation of current ripples in the region not affected by the initial disturbance in Fig. 3b. Both the qualitative and quantitative behaviors of the current and temperature distributions significantly differ from those observed in similar simulations performed on NbTi Rutherford cables [23].

A. 1-strand and 40-strand model results

A parametric set of simulations was performed to analyze the impact on the stability margin of the heat disturbance duration and of the spatial non-uniformity of the energy deposition, with 1-strand and N_s-strand approaches. The comparison between uniform and non-uniform heat deposition for the 40-strand model, at different fractions of the transport current, is presented in Fig. 4. To account for non-linear characteristics of the iron core, the magnetic flux density map was computed at each operation current level of interest; the minimal and maximal values of the magnetic flux density along each strand are reported in Tab III.

TABLE III
MAGNETIC FLUX DENSITY AS FUNCTION OF THE OPERATING CURRENT

I/I_{op}	B_{max} [T]	B_{min} [T]
100%	9.78	2.42
75%	7.48	1.85
50%	5.11	1.26
25%	2.63	0.65

For the simulations performed with non-uniform heat deposition, the mean value (about the 35% of the peak) of the energy disturbance has been reported. The pulse duration has been increased from 1 µs to 1 s to investigate both instantaneous and quasi steady-state heat depositions.

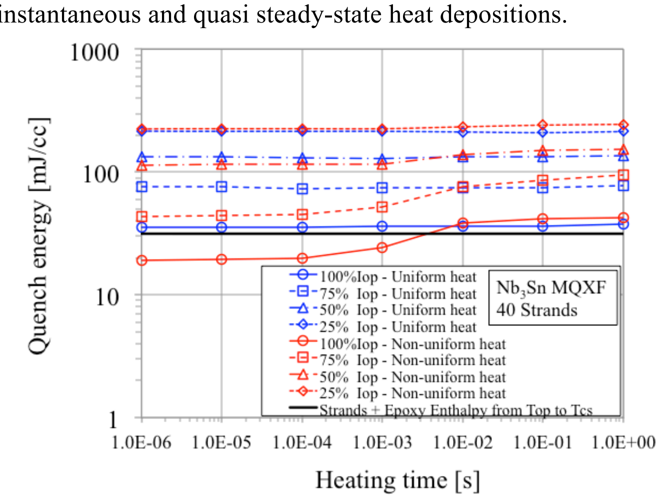

Fig. 4. Quench energy of the MQXF cable as a function of pulse duration at different transport currents computed with uniform and non-uniform heat distributions. The total available cable enthalpy at 100% I_{op} is also reported.

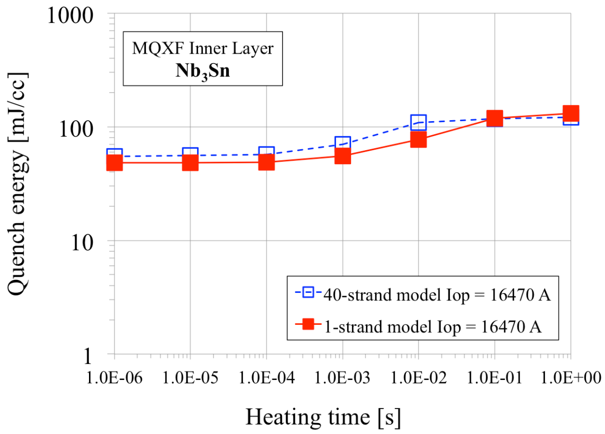

Fig. 5. Quench energy of the MQXF cable at the mid-plane as a function of pulse duration for the 1-strand and 40-strand model with non-uniform heat deposition.

The quench energy values are almost constant with pulse duration in the uniform deposition case, whereas they exhibit significant variations, especially for high values of pulse duration, in presence of a non-uniform heat deposition. With the same mean value of deposited energy, the non-uniform deposition results in a significant drop of the stability margin, for pulse durations less than 10 ms. This result shows that the Nb_3Sn cable is very sensitive to the non-uniformity of the heat deposition, thus indicating a strongly local behavior of the conductor. It is worth noting in Fig. 4 that the stability margin of the MQXF cable subjected to a uniform heat deposition is almost coincident with the cable enthalpy computed at the operating conditions, inclusive of strands and epoxy resin, calculated between T_{op} and T_{cs}. In this calculation, the epoxy resin only marginally contributes to the total enthalpy.

A comparison between the 1-strand and the 40-strand model is presented in Fig. 5. The values obtained with the two models are very similar, showing that the MQXF Nb_3Sn cable cannot take any significant advantage from the current and heat redistribution, especially at short pulse durations.

B. MQXF Nb_3Sn and MQ NbTi cables stability margin

The comparison between the quench energies of the MQXF Nb_3Sn and MQ NbTi cables is presented in Fig. 6, for the 1-strand model, and in Fig. 7 for the N_s-strand model.

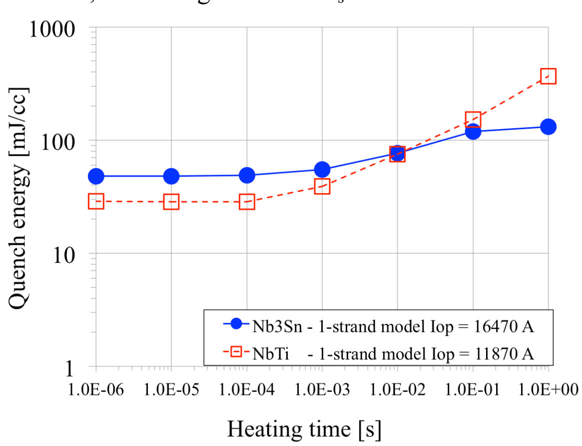

Fig. 6. Comparison between MQXF Nb3Sn and MQ NbTi cables. Quench energies as a function of pulse duration for the 1-strand model, with non-uniform heat deposition.

The results of the 1-strand model show that the quench energy of the MQXF Nb_3Sn cable is 70 % greater than that NbTi MQ at short pulse durations, due to the larger enthalpy available related to the greater temperature margin of the Nb_3Sn. This advantage is not found when considering the results of the N_s-strand model. In fact, the presence of the neighboring strands allows a better heat and current exchange in the NbTi MQ cable at short pulse durations, which determines a remarkable improvement of the stability margin. On the other hand, the MQXF cable does not exhibit any significant difference in quench energy when passing from the 1-strand to the 40-strand model. As a consequence, for short pulse durations the stability margin of the Nb_3Sn and NbTi cables are comparable. At high pulse durations, the stability margin of the NbTi conductor increases above the values obtained for the Nb_3Sn conductor. At long heating times, the NbTi cable can benefit from the presence of the helium bath more than the Nb_3Sn cable. This effect is related to a better heat exchange between the interstitial helium and the helium bath in the NbTi conductor, in contrast with the poor thermal contact between the insulating glass epoxy and the helium bath in the Nb_3Sn conductor.

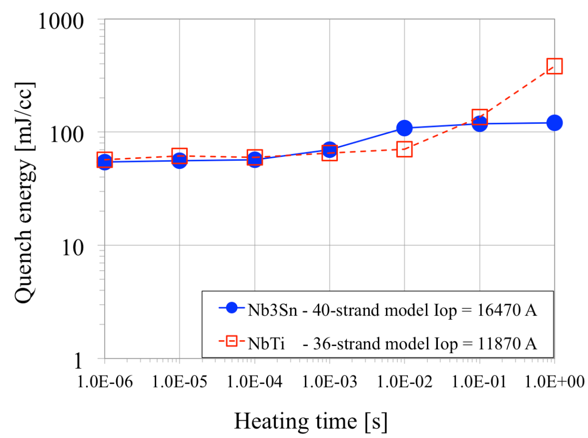

Fig. 7. Comparison between MQXF Nb3Sn and MQ NbTi cables. Quench energies as a function of pulse duration for the N_s-strand model, with non-uniform heat deposition.

Conclusion

This paper analyses the stability margin of the Nb_3Sn MQXF Rutherford cables for the High Luminosity Large Hadron Collider project at CERN, Switzerland. The cable has been modeled by a 1-D approach both with 1-strand and 40-strand model. The Nb_3Sn cables exhibit a local behavior in response to fast pulse durations, due to the limited current and heat exchange between neighboring strands which results in a very limited increase of quench energy from the *1-strand* to the *N-strand* model. The stability margin is therefore strongly affected by the details of the spatial distribution of the heat deposition. Despite the substantial differences between the Nb_3Sn MQXF and the NbTi MQ magnets, the simulations give quench energy values at short pulse durations very close to each other, especially at short pulse time durations.

REFERENCES

[1] L. Rossi, O. Brüning, "High Luminosity Large Hadron Collider A description for the European Strategy Preparatory Group", CERN-ATS-2012-236, 2012.

[2] E. Cavanna *et al*., "Design of the Nb3Sn Inner Triplet". FP7 High Luminosity Large Hadron Collider Design Study, 04 September 2015.

[3] L. Bottura, " Cable stability", CERN Yellow Report CERN-2014-005, pp.401-451, 2014.

[4] A. Valishev, et al., "Tevatron Accelerator Physics and Operation Highlights", Proceedings of PAC2011, New York, NY, USA, MOONCN2, p. 37–40, 2011.

[5] M. Bai, et al., "Beam-Losses and Beam-Induced Quenches at BNL", Proceedings of the 2014 Workshop on Beam-Induced Quenches, Geneva, Switzerland, 2014.

[6] J. B. Jeanneret, et al., "Quench Levels and Transient Beam Losses in LHC Magnets". LHC Project Report 044, 1996.

[7] H. Edwards, et al., "Measurements of Magnet Quench Levels by Proton Beam Spray", IEEE Transactions on Magnetics, MAG-13(1): 666–669, 1977.

[8] A. Priebe, "Quench tests of LHC magnets with beam: studies on beam loss development and determination of quench levels," Ph. D. Dissertation, Ecole Polytechnique Federale de Lausanne, Lausanne, Switzerland, 2014.

[9] M. Sapinski, et al., "Beam Induced Quenches of LHC Magnets", Proceedings of IPAC2013, Shanghai, China, THPEA045, p. 3243–3245, 2013.

[10] M. Sapinski, et al., "Beam-Induced Quench Tests of LHC Magnets. Proceedings of IPAC 2014, Dresden, Germany, MOOCB01, p. 52–54, 2014.

[11] K. Wittenburg, "Beam Losses and Machine Protection", AIP Conference Proceedings, Vol. 773, 2004.

[12] B. Auchmann *et al.*, "Testing Beam-Induced Quench Levels of LHC Superconducting Magnets", Phys. Rev. ST Accel. Beams 18, 061002, 2015.

[13] M. Breschi, A. Bevilacqua, L. Bottura, P. P. Granieri, "Analysis of Beam-Induced Quenches of the LHC Cables With a Multi-Strand Model", *IEEE Trans. Appl. Supercond.*, vol. 25 (3), 4700405, 2015.

[14] L. Bottura, C. Rosso, M. Breschi, "A General Model for Thermal, Hydraulic and Electric Analysis of Superconducting Cables," *Cryogenics*, vol. 40, pp. 617 – 626, 2000.

[15] P. Ferracin, et al., "Development of MQXF, the Nb3Sn Low-β Quadrupole for HiLumi LHC", *IEEE Trans. Appl. Supercond.*, vol. 26 (4), 4000207, 2016.

[16] S. Bermudez, "MQXF 2nd generation design" Joint HiLumi LHC-LARP

[17] L. Bottura, B. Bordini "J_c (B, T, ε) Parameterization for the ITER Nb_3Sn Production", *IEEE Trans. Appl. Supercond.*, vol. 19 (3), pp. 1521–1524, 2009.

[18] S. Russenschuck, "ROXIE - A Computer Code for the Integrated Design of Accelerator Magnets", CERN, Geneva, Switzerland.

[19] G. Battistoni *et al.*, "The FLUKA code: Description and bench-marking" in *Proc. AIP Conf. Hadron Shower Simul. Workshop,* vol. 896, pp. 31 – 49, 2007.

[20] A. Akhmetov, L. Bottura, M. Breschi, "A Continuum Model for Current Distribution in Rutherford Cables", *IEEE Trans. Appl. Supercond.*, vol. 11 (1), pp. 2138 – 2141, 2001.

[21] G. Willering, "Stability of superconducting Rutherford cables for accelerator magnets," PhD Thesis, University of Twente, The Netherlands, 2009.

[22] F. Grover, "Inductance Calculations: Working Formulas and Tables". New York: Van Nostrand, 1946.

[23] M. Breschi, A. Bevilacqua, L. Bottura, E. Felcini, "Stability modeling of the LHC NbTi Rutherford cables subjected to beam losses", submitted for publication on *Superconductor Science and Technology*, 2016.